Nonlocal plasma spectrum of graphene interacting with a thick conductor

Godfrey Gumbs,[1,2] Andrii Iurov,[1,3,*] and N. J. M. Horing[4]

[1]*Department of Physics and Astronomy, Hunter College of the City University of New York, 695 Park Avenue, New York, New York 10065, USA*
[2]*Donostia International Physics Center (DIPC), P de Manuel Lardizabal, 4, 20018 San Sebastian, Basque Country, Spain*
[3]*Center for High Technology Materials, University of New Mexico, Albuquerque, New Mexico 87106, USA*
[4]*Department of Physics and Engineering Physics, Stevens Institute of Technology, Hoboken, New Jersey 07038, USA*

A mean-field theory formalism is employed to analyze the nonlocal plasmon dispersion relation of monolayer graphene which is Coulomb coupled to a thick conductor. We calculate numerically the undamped plasmon excitation spectrum for arbitrary wave number. For gapped graphene, both the low-frequency (acoustic) and high-frequency (surface) plasmons may lie within an undamped opening in the particle-hole region. Furthermore, we find undamped plasmon excitations in a region of frequency-wave vector space which has no counterpart for free-standing gapped graphene.

PACS number(s): 73.21.−b, 71.70.Ej, 73.20.Mf, 71.45.Gm

I. INTRODUCTION

Recent research on plasmon excitations [1–4] has covered fundamental aspects such as nonlocality [5]; quantum effects in nanoscale structures, including fullerenes [6–8], graphene [9–12], carbon nanotubes [13–15], silicene [16,17], and metallic dimers [18]; surface plasmon lasing [19]; plasmon-electron interaction [20]; the potential role played by plasmon excitations in electronic sensors [21,22]; and radiation degradation of electronic and optoelectronic devices [23]. The surge in activity to understand and discover novel plasmonic materials is stimulated by possible applications such as light concentration for solar energy [24], devices for telecommunications [25], and near-field instrumentation [26]. Investigation of damped terahertz plasmons in graphene, interacting with surface plasmons of a substrate with heavy doping due to a large scattering rate, was addressed in Ref. [27]. The authors demonstrated that the field penetration of the graphene plasmons into the substrate is suppressed.

In view of the clear importance of achieving a detailed understanding of plasma excitations, we devote this paper to a specific area which has not been adequately covered so far in the literature. It concerns plasmon excitations in monolayer graphene. There are several papers dealing with calculations of the dispersion relation for monolayer graphene that is doped [9,11,28–30] as well as pristine graphene whose collective charge density oscillations are driven by temperature [31]. The work on gapped graphene [10] was partially motivated by the observation that when monolayer graphene is on a substrate such as boron nitride, an energy gap between the valence and conduction bands is produced, yielding a plasmon and single-particle excitation spectrum which can drastically differ from that of gapless monolayer graphene. In Refs. [9] through [10], the fundamental calculations of graphene polarizabilities were carried out for all frequencies and wavelengths. This fundamental formulation is brought to full fruition herein via a thorough investigation of the computationally challenging role of nonlocality in the plasmon spectrum of gapped as well as ungapped graphene, both free standing and at arbitrary height over a substrate, accounting for both plasma mode frequency and damping.

In a recent paper [32], it was demonstrated that high-frequency-plasmon excitations in graphene have a linear dispersion rather than a square-root dependence on wave vector. This unexpected result came as a surprise since theoretical calculations on free-standing graphene clearly do not yield a linear dependence in the long wavelength limit of plasmon excitations. An attempt was made to attribute this linear dependence of the plasmon frequency on wave vector to the local field corrections to the random-phase approximation. Horing [33] showed that when graphene is Coulomb coupled to a conductor, the surface plasmon causes the low-frequency π plasmon to have a linear dispersion. In the paper by Despoja *et al.* [34], the electronic excitations were calculated using time-dependent density functional theory. There, anisotropy and splitting of the π plasmons were found, as well as dispersive differences in the plasma spectrum, which seem to have been experimentally verified. However, so far these results have not been reproduced using an effective mass model.

Unlike three-dimensional bulk conductors and thick conducting materials with planar surfaces possessing bulk and surface plasmons, respectively, at finite frequency [35], two-dimensional (2D) inversion layers can sustain low-frequency collective modes. At these low energies, the plasmon excitations may contribute to a wide range of time-dependent processes leading to physisorption and chemisorption, for example. It has even been suggested that low-frequency plasmons might play a role in high-temperature superconductivity [36]. For these reasons, there has been considerable interest in these collective excitations both experimentally and theoretically and more recently in information transfer in nanostructures.

Recently, graphene was combined with prefabricated metamaterials and plasmonic nanoarrays, which led to the creation of tunable *hybrid* optical tools. Consequently, it is highly desirable to obtain detailed information about the behavior, especially the dispersion and damping of the plasmon modes of 2D layers interfaced with various types of substrates [37–40]. Also, we should mention some novel applications of graphene plasmonics to optics [41], microscopy [42], and nanolithography [43].

_____
*aiurov@chtm.unm.edu

In this paper, we calculate the full dispersion relation for undamped plasmons in a hybrid monolayer graphene-conductor structure. We apply nonlocal simulations to determine how the plasmon dispersion is affected when there is an energy gap between the valence and conduction bands, thereby generalizing the results in Ref. [10] where a surface is assumed to play a role.

The longitudinal excitation spectra of allowable modes will be determined from a knowledge of the frequency-dependent nonlocal dielectric function $\epsilon(\mathbf{r},\mathbf{r}';\omega)$ of the composite system, which depends on the position coordinates $\mathbf{r}$, $\mathbf{r}'$ and frequency ω. Alternatively, the normal modes correspond to the resonances of the inverse dielectric function $K(\mathbf{r},\mathbf{r}';\omega)$, satisfying $\int d\mathbf{r}'\, K(\mathbf{r},\mathbf{r}';\omega)\epsilon(\mathbf{r}',\mathbf{r}'';\omega) = \delta(\mathbf{r}-\mathbf{r}'')$. The significance of $K(\mathbf{r},\mathbf{r}';\omega)$ is that it embodies many-body effects [44,45] through screening by the medium of an external potential $U(\mathbf{r}';\omega)$ to produce an effective potential $V(\mathbf{r};\omega) = \int d\mathbf{r}'\, K(\mathbf{r},\mathbf{r}';\omega)U(\mathbf{r}';\omega)$. In Sec. II, we briefly review the formalism for calculating the inverse dielectric function for a 2D layer interacting with a semi-infinite conductor. Section III is devoted to an exhibition of our numerical results for the dispersion relations at arbitrary wavelength for this hybrid structure. We show explicitly how the gap for monolayer graphene affects both the dispersion relation for the surface plasmon and the low-frequency acoustic mode.

Specifically, we demonstrate that, due to the interaction with the substrate plasma, the low-frequency plasmon branch may exist undamped in a region of frequency–wave vector space that was not obtained for free-standing gapped graphene. We conclude with a summary of our results in Sec. IV.

II. GENERAL FORMULATION OF THE PROBLEM

In this work, we consider a composite nanoscale system consisting of a 2D layer separated from a thick dielectric material by a special gap. The 2D layer may be monolayer graphene [or a two-dimensional electron gas (2DEG) such as a semiconductor inversion layer or HEMT (high electron mobility transistor)]. The 2D graphene layer may have an energy gap, thereby broadening the applicability of the composite system model which also incorporates a separation layer and a semi-infinite plasma, as depicted in Fig. 1. The excitation spectra of allowable plasma modes will be determined from a knowledge of the nonlocal dielectric function $\epsilon(\mathbf{r},\mathbf{r}';\omega)$ which depends on position coordinates $\mathbf{r},\mathbf{r}'$ and frequency ω or
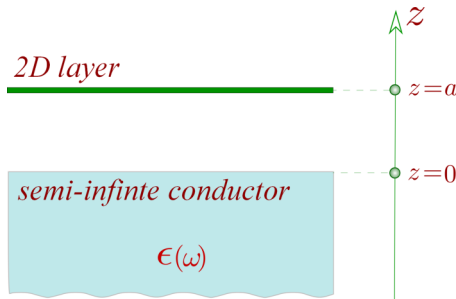

FIG. 1. (Color online) Schematic illustration of a thick (semi-infinite) metallic plasma interacting through the Coulomb force with a thin layer such as monolayer graphene at a distance a.

its inverse $K(\mathbf{r},\mathbf{r}';\omega)$ satisfying $\int d\mathbf{r}'\, K(\mathbf{r},\mathbf{r}';\omega)\epsilon(\mathbf{r}',\mathbf{r}'';\omega) = \delta(\mathbf{r},\mathbf{r}'')$. The field structure for $K(\mathbf{r},\mathbf{r}';\omega)$ is determined, using the technique of Ref. [33].

In operator notation, the composite dielectric function $\hat{\epsilon}$ and its inverse, $\hat{K} = \hat{\epsilon}^{-1}$, for the 2D layer and semi-infinite substrate is given by adding their polarizabilities $\hat{\alpha}_{2D}$ and $\hat{\alpha}_{SI}$, respectively, i.e.,

$$\hat{K}^{-1} = \hat{\epsilon} = \hat{1} + \hat{\alpha}_{SI} + \hat{\alpha}_{2D} \equiv \hat{\epsilon}_{SI} + \hat{\alpha}_{2D} = \hat{K}_{SI}^{-1} + \hat{\alpha}_{2D}. \quad (1)$$

Multiplication of Eq. (1) from the right by $\hat{K}$ and left by $\hat{K}_{SI}$ yields the basic random-phase approximation (RPA) integral equation

$$\hat{K} = \hat{K}_{SI} - \hat{K}_{SI}\hat{\alpha}_{2D}\hat{K}. \quad (2)$$

Additionally, $\hat{K}_{SI}$ is the inverse dielectric function for the semi-infinite substrate alone, whose surface lies in the $z = 0$ plane. In explicit integral form, after Fourier transforming with respect to coordinates parallel to the translationally invariant xy plane and suppressing the in-plane wave number $q_{\parallel}$ and frequency ω, we obtain

$$K(z_1,z_2) = K_{SI}(z_1,z_2)$$
$$- \int_{-\infty}^{\infty} dz' \int_{-\infty}^{\infty} dz''\, K_{SI}(z_1,z')\alpha_{2D}(z',z'')K(z'',z_2).$$
$$(3)$$

Here, the polarization function for the 2D layer is given by

$$\alpha_{2D}(z',z'') = \int_{-\infty}^{\infty} dz'''\, v(z',z''')D(z''',z''), \quad (4)$$

where v is the Coulomb potential energy and the 2D response function's localization to the layer at $z = a$ is expressed as

$$D(z''',z'') = \Pi_{2D}^{(0)}(q_{\parallel},\omega)\delta(z'''-a)\delta(z''-a), \quad (5)$$

with $\Pi_{2D}^{(0)}(q_{\parallel},\omega)$ as the 2D ring diagram of the RPA and for graphene is given by [9–12]

$$\Pi_{2D}^{(0)}(q_{\parallel},\omega) = \frac{gg'}{4\pi^2} \int d^2\mathbf{k}_{\parallel} \sum_{s,s'=\pm 1} F^{ss'}(\mathbf{q}_{\parallel},\mathbf{k}_{\parallel})$$
$$\times \frac{f_0(\varepsilon^s(k_{\parallel})) - f_0(\varepsilon^{s'}(|\mathbf{k}_{\parallel} + \mathbf{q}_{\parallel}|))}{\varepsilon^s(k_{\parallel}) - \varepsilon^{s'}(|\mathbf{k}_{\parallel} + \mathbf{q}_{\parallel}|) + \hbar(\omega + i0^+)} \quad (6)$$

with $\varepsilon^s(k_{\parallel})$ the energy dispersion for the conduction ($s = +$) and the valence ($s = -$), $g = 2$ denotes the valley degeneracy and $g' = 2$ the spin degeneracy. Also, $f^{(0)}(\epsilon_\alpha)$ is the occupation factor of the state $|\alpha\rangle = |\mathbf{q}_{\parallel},s\rangle$ determined by the Fermi-Dirac distribution function. We have $f_0(\epsilon_\alpha) = (\exp[(\epsilon_\alpha - \mu)/(k_B T)] + 1)^{-1}$ in terms of the chemical potential μ, Boltzmann's constant k_B, and temperature T. We have also introduced the form factor $F^{ss'}(\mathbf{q}_{\parallel},\mathbf{k}_{\parallel}) = |\langle\alpha|e^{i\mathbf{q}_{\parallel}\cdot\mathbf{r}}|\alpha'\rangle|^2$. Upon substituting this form of the polarization function for the monolayer into the integral equation for the composite inverse dielectric function K, we have

$$K(z_1,z_2) = K_{SI}(z_1,z_2) - \Pi_{2D}^{(0)}(q_{\parallel},\omega)$$
$$\times \int_{-\infty}^{\infty} dz'\, K_{SI}(z_1,z')v(z'-a)K(a,z_2). \quad (7)$$

We now set $z_1 = a$ in Eq. (7) and obtain

$$K(a,z_2) = K_{\text{SI}}(a,z_2) - \Pi_{2D}^{(0)}(q_{\|},\omega)$$

$$\times \left\{ \int_{-\infty}^{\infty} dz' \, K_{\text{SI}}(a,z')v(z'-a) \right\} K(a,z_2). \quad (8)$$

Solving algebraically for $K(a,z_2)$ yields

$$K(a,z_2) = \frac{K_{\text{SI}}(a,z_2)}{S_C(q_{\|},\omega)} \quad (9)$$

with the "dispersion factor" $S_C(q_{\|},\omega)$ given by

$$S_C(q_{\|},\omega) \equiv 1 + \Pi_{2D}^{(0)}(q_{\|},\omega) \left\{ \int_{-\infty}^{\infty} dz' \, K_{\text{SI}}(a,z')v(z'-a) \right\}, \quad (10)$$

whose zeros determine the plasmon resonances of the composite system. In our numerical calculations, we employ $K_{\text{SI}}(z,z')$ given by Eq. (30) of Ref. [45] for the semi-infinite metallic substrate in the local limit as follows:

$$K_{\text{SI}}(z,z';q_{\|},\omega)$$

$$= \theta(z) \left\{ \delta(z-z') + \delta(z')e^{-q_{\|}z} \left[\frac{1-\epsilon_B(\omega)}{1+\epsilon_B(\omega)} \right] \right\}$$

$$+ \theta(-z) \left\{ \frac{\delta(z-z')}{\epsilon_B(\omega)} + \delta(z')e^{q_{\|}z} \frac{1}{\epsilon_B(\omega)} \left[\frac{\epsilon_B(\omega)-1}{\epsilon_B(\omega)+1} \right] \right\}. \quad (11)$$

Equations (7) through (11) yield [33]

$$K(z_1,z_2) = K_{\text{SI}}(z_1,z_2) - \Pi_{2D}^{(0)}(q_{\|},\omega) \frac{K_{\text{SI}}(a,z_2)}{S_C(q_{\|},\omega)}$$

$$\times \left\{ \int_{-\infty}^{\infty} dz' \, K_{\text{SI}}(z_1,z')v(z'-a) \right\} \quad (12)$$

with

$$S_C(q_{\|},\omega) = 1 + \frac{2\pi e^2}{\epsilon_s q_{\|}} \Pi_{2D}^{(0)}(q_{\|},\omega) \left\{ 1 + e^{-2q_{\|}a} \frac{1-\epsilon_B(\omega)}{1+\epsilon_B(\omega)} \right\}. \quad (13)$$

Here we have defined $\epsilon_s = 4\pi\epsilon_0\epsilon_b$, where ϵ_0 is the permeability of free space and ϵ_b is the background dielectric constant. Also, $\epsilon_B(\omega) = 1 - \omega^2/\omega_p^2$ with ω_p standing for the bulk plasma frequency.

Although the principal focus here is to examine the role of 2D graphene plasma nonlocality embedded in $\Pi_{2D}^{(0)}(q_{\|},\omega)$ on the coupled plasmon spectrum of the composite system, we briefly revisit the local results of Ref. [33] to point out their generalization to include gapped graphene along with the previously discussed gapless results. In this regard, the graphene polarizability is also taken in the local limit with $\Pi_{2D}^{(0)}(q_{\|},\omega) \approx Cq_{\|}^2/\omega^2$ so Eq. (13) yields

$$1 - \frac{2\pi Ce^2}{\epsilon_s\omega^2}q_{\|} \left\{ 1 + e^{-2aq_{\|}} \frac{\omega_p^2}{2\omega^2 - \omega_p^2} \right\} = 0, \quad (14)$$

where the inclusion of a gap is described by [10]

$$C = \frac{2\mu}{\pi\hbar^2} \left\{ 1 - \frac{\Delta^2}{\mu^2} \right\}, \quad (15)$$

where μ is the chemical potential and Δ is the gap between valence and conduction bands. Consequently, Eq. (14) yields the local plasmon frequency as follows [33]:

$$\omega^2 = K_1 \pm \sqrt{K_2}, \quad (16)$$

with K_1 and K_2 defined by

$$K_1 = \frac{\pi e^2 C}{\epsilon_s}q_{\|} + \left(\frac{\omega_p}{2}\right)^2$$

$$K_2 = \frac{\pi e^2 C \,\omega_p^2}{\epsilon_s}e^{-2aq_{\|}}q_{\|} + \left[\left(\frac{\omega_p}{2}\right)^2 - \frac{Ce^2\pi}{\epsilon}q_{\|} \right]^2. \quad (17)$$

In the low-wave-number limit $q_{\|} \ll 1/a$ these expressions are reduced to:

$$\omega_1 \approx 2e\sqrt{\frac{\pi aC}{\epsilon_s}}q_{\|}$$

$$\omega_2 \approx \frac{\omega_p}{\sqrt{2}} + \frac{\sqrt{2}\pi Ce^2}{\epsilon_s\omega_p}q_{\|}, \quad (18)$$

which are both linear in $q_{\|}$, differing from the $q_{\|}^{1/2}$ dependence for free-standing graphene or the 2DEG [9–11,46–49].

Nonlocality of the graphene plasma introduces changes in the features of $K(z_1,z_2)$ of Eq. (12) and in its coupled 2D-surface plasmon spectrum in two respects. First, the local coupled mode spectrum described in the preceding paragraph is modified by nonlocality corrections in Eq. (13) with the use of the polarization function $\Pi_{2D}^{(0)}(q_{\|},\omega)$ for all wave numbers as calculated in Ref. [10] for gapped graphene. Second, nonlocality introduces natural damping through the occurrence of regions in which plasmons can decay into electron-hole pairs [50] consistent with energy-momentum conservation. The intersection of the plasmon dispersion curve $\omega(q_{\|})$ with such a particle-hole excitation region (PHER) signals the onset of damping at $T = 0\,K$, with $\text{Im}S_C(q_{\|},\omega) \neq 0$. However, it is the undamped coupled plasmons that are of interest with

$$\text{Im}S_C(q_{\|},\omega) = \text{Im}\left[\Pi_{2D}^{(0)}(q_{\|},\omega)\right] \frac{2\pi e^2}{\epsilon_s q_{\|}}$$

$$\times \left\{ 1 + e^{-2q_{\|}a} \frac{1-\epsilon_B(\omega)}{1+\epsilon_B(\omega)} \right\} = 0. \quad (19)$$

The features of the interacting graphene-surface plasmon spectrum are analyzed here numerically using the real and imaginary parts of the polarizabilities of B. Wunsch [9] as well as Hwang and Das Sarma [11] for gapless graphene and Pyatkovskiy [10] for gapped graphene (all at zero temperature).

In regard to the mechanism of damping, the procedure used in our numerical calculations treats metallic surface plasmons in the local limit, while the acoustic plasmon attributed to the graphene layer was taken into consideration nonlocally with the inclusion of its Landau damping. This is reasonable because the high-frequency surface plasmon is not Landau damped by single-particle excitations arising from the metallic substrate over a wide wave number range for $q \lesssim 1/\lambda_F$, in which the Fermi wavelength in metals is comparable with the lattice constant $\lambda_F \simeq 0.5$ nm. To be clear, we point out that this Landau damping from the substrate can be broken

down into two contributions (see Eqs. (28)– (30) of Ref. [45]). The one corresponding to particle-hole excitations which were included when an integration was executed over q_z to obtain the inverse dielectric function for the SI substrate. The second contribution comes through damping in the ω-$q_\parallel$ plane from bulk single-particle excitations (SPE's). We took the local limit which is reasonable since the damping arising from the SPE's within the 2D layer is dominant compared to the bulk SPE's as the carrier density in the substrate is high. Correspondingly, within the range of validity it is sufficient to neglect plasmon damping originating from the conducting half-space, confining our attention to Landau damping from the 2D layer. Our calculations are carried out to complement the already-published works of Refs. [9–11] and others, all of whom considered only Landau damping from the monolayer to the exclusion of other damping mechanisms. It also follows from our numerical simulations that our model yields both the intensity and energy dispersion of the plasmon modes, which are in agreement with recent experimental data [51,52]. Our model thus seems reasonable for sufficiently clean samples. Damping due to finite-temperature effects could also be of interest [12].

If the band gap in graphene is opened due to the presence of a substrate, this might lead to the existence of significant plasmon damping other than Landau damping. However, the interaction with a substrate is not the only way to create an energy band gap in graphene. A band gap of up to $\Delta \simeq 117$ meV could be achieved by exposing graphene to a laser-generated circularly polarized electromagnetic field. In this regard, we would like to mention a paper by Kibis [53]. A theory for the polarization function, plasmon dispersion, and damping was reported in Ref. [54]. In connection with an investigation of strong non-Landau damping, we also mention Ref. [55], in which an analytical model for coupled exciton-plasmon states was presented. However, that model differs substantially from ours, mainly because of the coupling between the plasmon in graphene and the excitons in a narrow gap semiconductor quantum wells.

III. CALCULATED RESULTS AND DISCUSSION

First, we consider graphene with no energy gap and linear energy dispersion for the valence and conduction bands. The boundaries of the particle-hole modes region are linear, enclosing a triangular region, where the plasmons are not damped. The plasmons for gapless graphene are shown in Fig. 2. We discern two plasmon branches, one attributed to the surface (the upper branch, originating from $\omega_p/\sqrt{2}$ frequency) and the other due to the graphene sheet (starting at the origin). We present results for various values of the distance a between the layer and the surface. When this separation is increased, the two branches evolve into a merged spectral line, similarly to the plasmon of extrinsic gapless graphene. The surface plasmon branch tends to be dispersionless and to exist in the long-wavelength limit only. For all presented cases, the upper plasmon mode shows a stronger and broader peak. We display the absolute value of the real part of $S_C^{-1}(q_\parallel,\omega)$ to emphasize each peak.

We also solve the equation $\mathrm{Re}\,S_C(q_\parallel,\omega) = 0$ numerically, demonstrating the exact solution for the plasmon dispersion
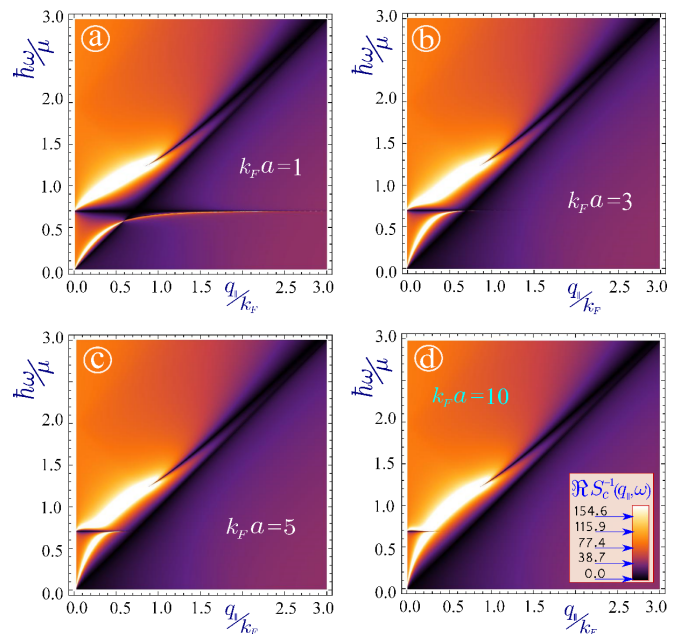

FIG. 2. (Color online) Density plots of the real part of the inverse of the dispersion factor $S_c(q_\parallel,\omega + i0^+)$ for extrinsic (doped) graphene with no band gap ($\Delta = 0$): peaks correspond to the plasmon resonances. Panels (a)–(d) demonstrate the plasmon spectrum for various separations between the graphene layer and the surface, $a = 1, 3, 5,$ and $10 k_F^{-1}$, where k_F is the Fermi wave number.

relation for both cases of zero (see Fig. 3) and finite (Fig. 4) energy band gap. These solutions become extremely interesting when the upper branch splits into two parts for the case of the small energy gap. When the gap is zero, once again we see that the upper branch (which we attribute to the presence of a surface) adopts certain features of the plasmon in gapless
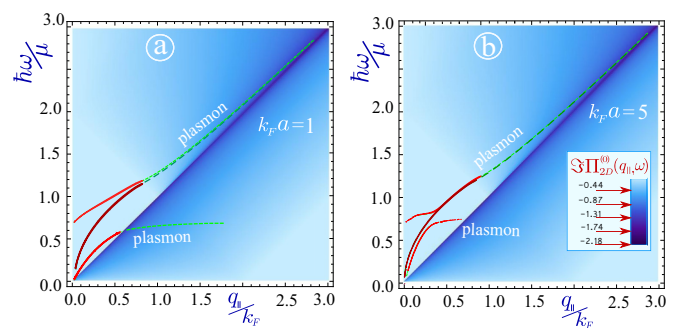

FIG. 3. (Color online) Exact numerical solutions for the plasmon dispersion of gapless graphene. The highest and lowest curves are the solutions of the plasmon dispersion equation $\mathrm{Re}\,S_C(q_\parallel,\omega) = 0$ for graphene at a distance $a = k_F^{-1}$ from a conducting surface, whereas the curve in between these two solutions corresponds to the zeros of $1 + 2\pi e^2/(\epsilon_s q_\parallel)\mathrm{Re}\,\Pi_{2D}^{(0)}(q_\parallel,\omega) = 0$ for free-standing graphene. Panel (a) corresponds to a smaller distance between the layer and the surface $a = k_F^{-1}$, whereas panel (b) demonstrates the case when $a = 5k_F^{-1}$ In both (a) and (b), the plasmon energy is scaled with respect to the chemical potential μ and we superimpose all plasmon curves on a background of a density plot of $\mathrm{Im}\,\Pi_{2D}^{(0)}(q_\parallel,\omega)$ to illustrate the effects due to Landau damping.
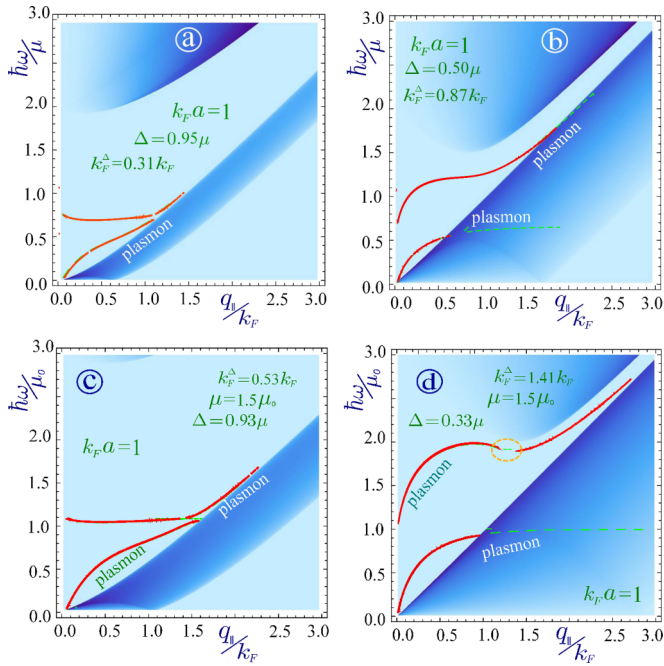
FIG. 4. (Color online) Exact numerical solutions of $\mathrm{Re}\,S_C(q_\parallel,\omega+i0^+)=0$ for gapped graphene at a distance $a=k_F^{-1}$ from a conducting surface. The plasmon excitation spectrum is superimposed on a background showing the density plot of $\mathrm{Im}\,\Pi_{2D}^{(0)}(q_\parallel,\omega+i0^+)$ whose values determine Landau damping. The red lines correspond to undamped plasmons when the magnitude of the plasmon dispersion factor $|S_C(q_\parallel,\omega+i0^+)|$ vanishes. Panels (a) and (b) show the case of $\Delta=0.95$ and 0.5, and panels (c) and (d) demonstrate the behavior of the plasmon spectra for $\mu=1.5\,\mu_0$ and $\Delta=0.93\,\mu$ and $\Delta=0.33\,\mu$, respectively. Here $\mu_0=0.2$ eV is the chemical potential used in the calculations of Fig. 3. This value for μ_0 is chosen to ensure the applicability of isotropy of the energy band structure at low doping [30]. Also, in our notation, $k_F^\Delta\equiv\sqrt{\mu^2-\Delta^2}/(\hbar v_F)$.

graphene mainly because the branch is located in the same $\{\omega,q_\parallel\}$ regions, both inside and outside the PHER. However, according to our analytical results, for long wavelengths both branches possess finite slope, in contrast to $\sim\sqrt{q_\parallel}$ behavior in free-standing graphene.

The case of a small energy gap is presented in Fig. 4 for various energy gap and doping values. Similar to free-standing graphene, the upper branch is extended due to splitting of the PHER. It might also be split into two different branches as mentioned in Ref. [10]. When the distance a of the 2D layer from the surface is increased, the two plasmon branches merge into a single branch, which is similar to the plasmon dispersion in gapped free-standing graphene. The general conclusion is that when one of the factors (energy gap, chemical potential, or the separation a) is appreciable, the changes caused by a sizable change in one of the others is not significant.

The role played by the energy band gap is an important part of our investigation. For monolayer graphene, an energy gap leads to to an extended region of undamped plasmons [10]. In Fig. 5, we present the regions of the real and imaginary parts of the noninteracting polarization function which have distinct functional forms. We pay particular attention to the regions
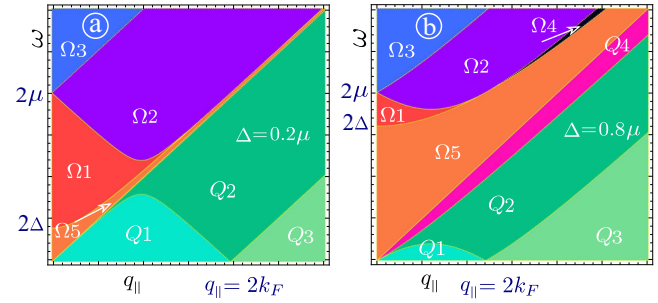

FIG. 5. (Color online) Schematics showing the regions having differing analytic expressions for the noninteraction polarization function $\Pi_{2D}^{(0)}(q_\parallel,\omega)$. Each part (real or imaginary) is determined by a different analytic expression, as in Refs. [10,16,17]. The regions with $\omega>\hbar v_F q_\parallel$ are presented as $\Omega1$–$\Omega5$, while the opposite are given by $Q1$–$Q4$. Regions with nonzero $\mathrm{Im}\,\Pi_{2D}^{(0)}(q_\parallel,\omega)$ are $\Omega1$, $\Omega5$, $Q4$ (where undamped plasmons exist), and $Q3$. Panel (a) demonstrates the case of a small band gap $\Delta=0.2\,\mu$, whereas panel (b) shows the case of relatively large gap $\Delta=0.6\,\mu$.

outside of the single-particle excitation continuum since, as mentioned previously, they encompass plasmon frequencies in the domains of $\{\omega,q_\parallel\}$ in which the plasmons are not damped. We denote these planar regions ($\Omega1$, $\Omega5$, and $Q4$) with reddish colors. The condition $\mathrm{Im}\,\Pi_{2D}^{(0)}(q_\parallel,\omega)=0$ is also satisfied in $Q3$, but no plasmons are observed in this region. Region $Q4$ with $\hbar v_F q_\parallel>\omega$ plays a crucial role in our study because this is where the extended undamped lower plasmon branch is located. This is a new finding, which was not encountered in previous works of Refs. [9–12,28] and it is attributed to screening by the carriers in the thick substrate adjoining the 2D layer.

Figure 6 exhibits our results for plasmon excitations of a composite system consisting of a layer of gapped graphene and a thick substrate for various values of the energy gap, chemical potential, and the distance between the two bodies. The PHER and its boundaries constitute an important factor determining the plasmons. Consequently, the upper branch, located mainly in regions $\Omega1$ and $\Omega5$, bears some similarity to the plasmons in free-standing gapped graphene, including its splitting into two parts in the vicinity of the boundary of $\Omega2$. The results for both the lower and upper branches definitely depend on the gap. In the long-wavelength limit, we demonstrate that $\omega_1\simeq\sqrt{C}$ and $\omega_2\simeq\omega_p/\sqrt{2}+\cdots\simeq C$, where $C\simeq(1-\Delta^2/\mu^2)$. The plasmon dispersion relation for a free-standing graphene layer with a finite energy gap is $\omega\simeq\sqrt{Cq_\parallel}$, which differs from our solution and that in Ref. [33]. However, there is an interesting similarity in that the plasmon frequency is decreased with increased energy gap. This dependence is observed for increased values of $q_\parallel$.

The important differences in the plasmon spectra between free-standing graphene and graphene interacting with a half space arise from the lower plasmon branch which lies on both sides of the straight line $\omega=v_F q_\parallel$ and has a linear dispersion for small $q_\parallel$. According to previously published results [10], the size of the $Q4$ region is determined by doping as well as the energy gap. The boundary between $Q4$ and $Q2$ [with finite $\mathrm{Im}\,\Pi_{2D}^{(0)}(q_\parallel,\omega)$] is described by
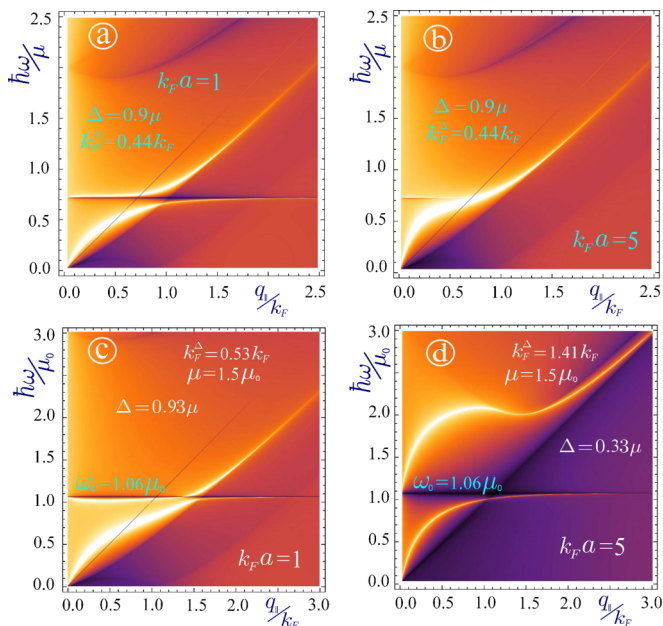
FIG. 6. (Color online) Density plot of the real part of the inverse dispersion function $S_c(q_\parallel,\omega)$ for extrinsic (doped) graphene when the band gap is finite and where its peak positions correspond to the plasmon frequencies. The results in the panels were obtained for various chosen values of the energy gap Δ, the distance a between the surface and the graphene layer and the chemical potential μ, so panel (a) shows the case when $k_F a = 1$ and $\Delta = 0.6\,\mu$, (b) $k_F a = 5$ and $\Delta = 0.6\,\mu$, (c) $\mu = 1.5\,\mu_0$, $k_F a = 1$, and $\Delta = 0.93\,\mu$, and (d) $\mu = 1.5\,\mu_0$, $k_F a = 1$, and $\Delta = 0.33\,\mu$. In our notation, μ_0 is an arbitrary doping, parameter in terms of which we measure chemical potential. We introduced $k_F^\Delta \equiv \sqrt{\mu^2 - \Delta^2}/(\hbar v_F)$.
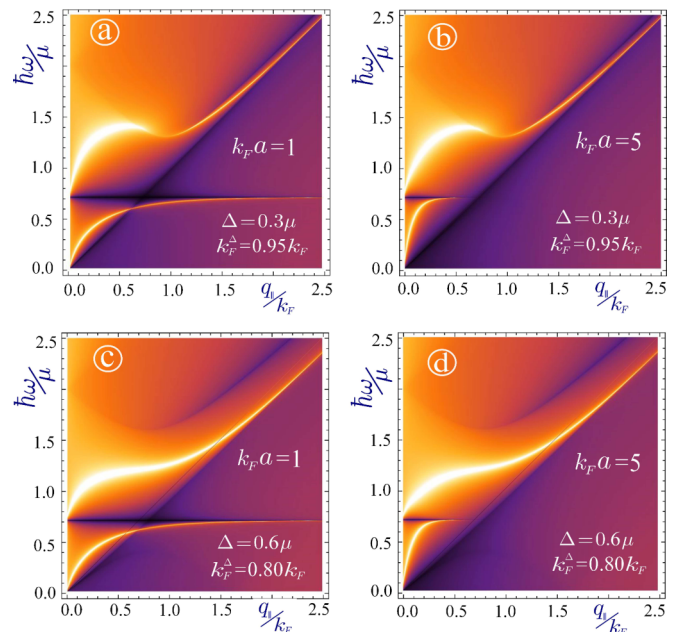

FIG. 7. (Color online) Density plot of the real part of the inverse dispersion factor $S_c(q_\parallel,\omega + i0^+)$ for extrinsic (doped) graphene having a finite band gap ($\Delta \neq 0$) with the peaks corresponding to the plasmons. The panels are for various values of the energy gap Δ and distance a between the surface and the graphene layer. Panel (a) shows the case when $a = k_F^{-1}$ and $\Delta = 0.3\,\mu$, (b) $a = 5k_F^{-1}$ and $\Delta = 0.3\,\mu$, (c) $a = k_F^{-1}$ and $\Delta = 0.6\,\mu$, and (d) describes $a = 5k_F^{-1}$ and $\Delta = 0.6\,\mu$. We define $k_F^\Delta \equiv \sqrt{\mu^2 - \Delta^2}/(\hbar v_F)$.

$\omega = -\mu + \sqrt{(\hbar v_F)^2(q_\parallel + k_F)^2 + \Delta^2}$ with $\hbar v_F k_F = \sqrt{\mu^2 - \Delta^2}$. For $\Delta = 0$, this boundary line is reduced to $\omega = v_F q_\parallel$. The plasmon dispersion for various doping concentrations is presented in Fig. 6. Increasing both μ and Δ, we find more extended branches where undamped plasmons exist. Figure 6(d) clearly demonstrates *anticrossing* and an extended region of undamped plasmons for both branches. In all cases, the lower plasmon branch does not rise above the line $\omega = \omega_p/\sqrt{2}$. The curvature of the upper branch is determined by the ratio Δ/μ rather rather than by the gap itself. For certain values of this ratio, the upper branch consists of two different, separated plasmon branches.

We note that the exact numerical solutions in Fig. 4 corresponding to $\mathrm{Re}\,S_C(q_\parallel,\omega) = 0$ are in agreement with the data for the density plots in Figs. 7 and 6. The results in these plots confirm the anticrossing and the extension of the lower plasmon branches with increased doping and energy gap. We also note that for large values of the ratio $\Delta/\mu \geqslant 0.9$ the lower branch becomes nearly dispersionless.

We now consider in detail the case for a layer closely located to a surface. This is relevant to recent experiments conducted by Politano *et al.* [37,51,52]. Our numerical results are presented in Fig. 8. They demonstrate that if the distance between the surface and the layer becomes less than some critical value a_c, the lower acoustic plasmon branch becomes overdamped. This is similar in nature to the experimentally

obtained data. We note that since the imaginary part of the polarization function for gapless graphene is nonzero below the diagonal ($\sim q_\parallel^2 \theta(v_F q_\parallel - \omega)/\sqrt{|\omega^2 - v_F^2 q_\parallel^2|}$), the acoustic plasmon is damped only if it lies below the diagonal $\Omega_d = v_F q$ for $q_\parallel \to 0$. The critical distance is determined as $a_c = \epsilon_s v_F^2/(4\pi e^2 C)$ for the zero-energy gap.

Also, we would like to mention that if a plasmon branch is located below the main diagonal $\Omega_d = v_F q$, and the plasmon is overdamped, one can no longer separate the real and imaginary parts of the plasmon frequency, since the correction to the real frequency coming from the higher even powers of the imaginary frequency (such as γ^2, where $\gamma = \mathrm{Im}\,\omega$) and the higher powers in $q_\parallel$ are no longer a small parameter. Consequently, one cannot find a real plasmon dispersion using the analytical formulas for the polarization provided in Refs. [9–12].

In general, the energies of surface states lie within the gap of a bulk crystal energy band structure. Consequently, these states are characterized by an imaginary wave number which leads to an exponential decay into the bulk. However, the imaginary wave vector plays no role here because we use the local limit in approximating the inverse dielectric function for a semi-infinite medium which is represented by the jellium model. Furthermore, the in-plane wave vector is always real and the plasmon may lose energy due to Landau damping. For this, we calculated *both* real and imaginary parts of the inverse dielectric function in our numerical simulations.
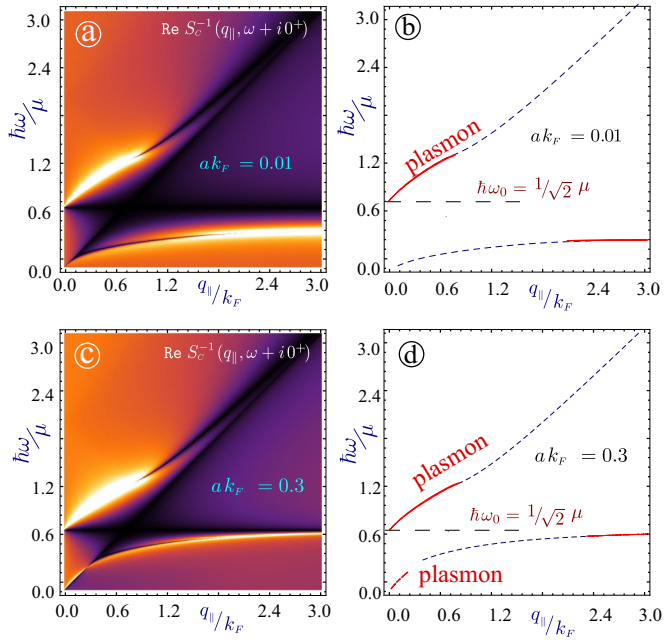
FIG. 8. (Color online) Plasmons for a closely located layer and surface. The left panels (a) and (c) demonstrate the density plots for a real part of the inverse dispersion function $S_c^{-1}(q_{\parallel}, \omega + i0^+)$ for extrinsic (doped) graphene with no band gap ($\Delta = 0$) with the peaks corresponding to the plasmon resonances. The right panel shows the corresponding exact numerical solutions for the plasmon branches (both damped and undamped). While the upper panels (a) and (b) show the case of extremely small distance between the layer and the semi-infinite conductor $a = 0.01k_F^{-1}$ with the lower plasmon branch damped, the lower panels (c) and (d) correspond to a critical value $a_c \simeq 0.3k_F^{-1}$ of the distance, when the undamped acoustic plasmon branch still exists for $q \to 0$. Technically, the lower acoustic branch now consists of two separated plasmons.

IV. CONCLUDING REMARKS

In summary, we have calculated the nonlocal plasmon dispersions within RPA for monolayer graphene interacting with a substrate for arbitrary wavelengths. In this, we investigated numerically the effects of the energy gap for extrinsic graphene, as well as the effects of its distance from the surface, on the plasmon dispersion relation. Our considerations were motivated by recent experimental work showing a linear plasmon dispersion in the long-wavelength limit [52] and the earlier theoretical work by one of the authors [33] to account for this observation, which is extended here to a fully general numerical description of nonlocal effects in monolayer graphene when the separation a is varied and when the energy gap is increased. Our new results in this paper vividly demonstrate that a thorough investigation necessitates incorporating the polarization into the dispersion equation at shorter wavelengths.

It should be emphasized that we have found an important region devoid of Landau damping for the coupled plasmons, which was previously unrecognized. This could be achieved by careful and extensive numerical simulations. Our results on the split plasmon branches due to a depolarization shift arising from the layer-substrate coupling and represent an

interesting feature in the excitation spectrum. In this respect, exact numerical solutions played a crucial role. As a matter of fact, most of our data were obtained within the framework of carrying out numerical experiments and could not have been predicted theoretically based only on an analytic formalism. Demonstration of the extended regions of undamped plasmons is a key result. Furthermore, as we discussed, its existence can expand the applicability of plasmon mode excitations to applications in optoelectronics, for example. Apart from all the above-mentioned results, there is another finding which deserves mentioning. When the thick conductor and 2D layer are not coupled, we normally obtain two plasmon branches, associated with the 2D layer (acoustic plasmon, starting at the origin) and the other branch is associated with the surface plasmon, originating at $\omega_p/\sqrt{2}$. If the Coulomb interaction between the layer and the conductor is sufficiently strong and an energy band gap is introduced, the upper "surface" plasmon acquires interesting features (being either damped or undamped, depending on the energy gap; for certain gap values it could be divided into two undamped branches), as it was reported for graphene. So the plasmon branches are hybridized, and the surface plasmon branch is significantly affected by the layer. Finally, if the distance between the layer and the surface is decreased $a < 0.3$ nm, our model faithfully reproduces the finding recently reported experimentally in the papers [37,51,52]. Our theory, in conjunction with the numerics, can provide an explanation for the data, reported for the plasmon frequencies, their intensity, and damping, and to predict other potential experimental features.

The distance a between monolayer graphene and the surface was varied in our nonlocal numerical calculations. In all cases, there are two plasmon branches; one originating from the surface plasmon and the other from the graphene layer. Both gapless and gapped graphene have been investigated. The most important consequence of introducing the energy gap in graphene is the extended region of undamped plasmons for both branches. Specifically, referring to Fig. 3(a), we note that the upper plasmon dispersion curve enters the gap in the particle-hole spectrum like that for gapped free-standing graphene and these two curves are close to each other within this gap. In addition, the lower plasmon branch is undamped for a wider range of wave vectors $q_{\parallel}$ by entering the gap in the particle-hole region. As revealed in Fig. 4(c), the lower branch may anticross with the upper one for sufficiently high doping concentration and large band gap. Both plasmon frequencies decrease with increased energy gap. This is also the behavior for free-standing gapped graphene. However, the exact functional dependence differs in each case. Also, either one of the plasmon branches may bifurcate into two branches in the the single-particle excitation region, as demonstrated in Fig. 6(b). These new results for the plasmons may potentially lead to a number of applications in electronic devices since the plasmons play an important role in the response properties to external electromagnetic fields.

[1] A. H. Castro Neto, F. Guinea, N. M. R. Peres, K. S. Novoselov, and A. K. Geim, Rev. Mod. Phys. **81**, 109 (2009).

[2] D. S. L. Abergela, V. Apalkov, J. Berashevicha, K. Ziegler, and Tapash Chakraborty, Adv. Phys. **59**, 261 (2010).

[3] Luis E. F. Foa Torres, Stephan Roche, and Jean-Christophe Charlier, *Introduction to Graphene-Based Nanomaterials: From Electronic Structure to Quantum Transport* (Cambridge University Press, Cambridge, 2014).

[4] G. Gumbs and D. H. Huang, *Properties of Interacting Low-Dimensional Systems* (Wiley-VCH Verlag GmbH & Co. KGaA, Boschstr, Weinheim, 2011).

[5] D. H. Huang, Godfrey Gumbs, and S.-Y. Lin, J. Appl. Phys. **105**, 093715 (2009).

[6] G. Gumbs, A. Iurov, A. Balassis, and D. H. Huang, J. Phys.: Condens. Matter **26**, 135601 (2014).

[7] Andrii Iurov, Godfrey Gumbs, Bo Gao, and Danhong Huang, Appl. Phys. Lett. **104**, 203103 (2014).

[8] Antonios Balassis and Godfrey Gumbs, Phys. Rev. B **90**, 075431 (2014).

[9] B. Wunsch, T. Stauber, F. Sols, and F. Guinea, New J. Phys. **8**, 318 (2006).

[10] P. K. Pyatkovskiy, J. Phys.: Condens. Matter **21**, 025506 (2009).

[11] E. H. Hwang and S. Das Sarma, Phys. Rev. B **75**, 205418 (2007).

[12] S. Das Sarma and Q. Li, Phys. Rev. B **87**, 235418 (2013).

[13] M. F. Lin and K. W. Shung, Phys. Rev. B **50**, 17744 (1994).

[14] Y. Wang, X. Wang, Q. Wu, X. J. He, T. L. Gui, and Y. J. Tong, Plasmonics **7**, 411 (2012).

[15] R. Saito, G. Dresselhaus, and M. S. Dresselhaus, *Physical Properties of Carbon Nanotubes* (Imperial college press, London, 1998), Vol. 4.

[16] Cheng-Cheng Liu, Wanxiang Feng, and Yugui Yao, Phys. Rev. Lett. **107**, 076802 (2011).

[17] C. J. Tabert and E. J. Nicol, Phys. Rev. B **89**, 195410 (2014).

[18] P. Nordlander, C. Oubre, E. Prodan, K. Li, and M. I. Stockman, Nano Lett. **4**, 5 (2004).

[19] D. Bergman and M. Stockman, Phys. Rev. Lett. **90**, 027402 (2003).

[20] C. Tegenkamp, H. Pfnür, T. Langer, J. Baringhaus, and H. W. Schumacher, J. Phys.: Condens. Matter **23**, 012001 (2011).

[21] K. A. Willets and R. P. Van Duyne, Annu. Rev. Phys. Chem. **58**, 267 (2007).

[22] Godfrey Gumbs, Andrii Iurov, and Danhong Huang, arXiv:1410.2851 [cond-mat.mtrl-sci].

[23] P. Sigmund, *Particle Penetration and Radiation Effects* (Springer-Verlag, Berlin, 2006).

[24] S. Pillai, F. J. Beck, K. R. Catchpole, Z. Ouyang, and M. A. Green, J. Appl. Phys. **109**, 073105 (2011).

[25] I. Goykhman, B. Desiatov, J. Khurgin, J. Shappir, and U. Levy, Nano Lett. **11**, 2219 (2011).

[26] Wei Bao, Matteo Staffaroni, Jeffrey Bokor, Miquel B. Salmeron, Eli Yablonovitch, Stefano Cabrini, Alexander Weber-Bargioni, and P. James Schuck, Opt. Express **21**, 8166 (2013).

[27] A. Satou, Y. Koseki, V. Ryzhii, V. Vyurkov, and T. Otsuji, arXiv:1401.3396 [cond-mat.mtrl-sci].

[28] K. W.-K. Shung, Phys. Rev. B **34**, 979 (1986).

[29] O. Roslyak, G. Gumbs, and D. H. Huang, J. Appl. Phys. **109**, 113721 (2011).

[30] M. Pisarra, A. Sindona, P. Riccardi, V. M. Silkin, and J. M. Pitarke, New J. Phys. **16**, 083003 (2014).

[31] S. Das Sarma and A. Madhukar, Phys. Rev. B **23**, 805 (1981).

[32] C. Kramberger, R. Hambach, C. Giorgetti, M. H. Rmmeli, M. Knupfer, J. Fink, B. Bchner, L. Reining, E. Einarsson, S. Maruyama, F. Sottile, K. Hannewald, V. Olevano, A. G. Marinopoulos, and T. Pichler, Phys. Rev. Lett. **100**, 196803 (2008).

[33] N. J. M. Horing, Phys. Rev. B **80**, 193401 (2009).

[34] V. Despoja, D. Novko, K. Dekanic, M. Sunjic, and L. Marusic, Phys. Rev. B **87**, 075447 (2013).

[35] R. H. Ritchie, Phys. Rev. **106**, 874 (1957).

[36] Bogdan Diaconescu, Karsten Pohl, Luca Vattuone, Letizia Savio, Philip Hofmann, Vyacheslav M. Silkin, Jose M. Pitarke, Eugene V. Chulkov, Pedro M. Echenique, Daniel Farias, and Mario Rocca, Nature **448**, 57 (2007).

[37] A. Politano and G. Chiarello, Nanoscale **6**, 10927 (2014).

[38] G. Giovannetti, P. A. Khomyakov, G. Brocks, V. M. Karpan, J. van den Brink, and P. J. Kelly, Phys. Rev. Lett. **101**, 026803 (2008).

[39] K. L. Grosse, M.-H. Bae, F. Lian, E. Pop, and W. P. King, Nat. Nanotech. **6**, 287 (2011).

[40] N. Reckinger, A. Vlad, S. Melinte, J. F. Colomer, and M. Sarrazin, Appl. Phys. Lett. **102**, 211108 (2013).

[41] A. V. Zayats, I. I. Smolyaninov, and A. A. Maradudin, Phys. Rep. **408**, 131 (2005).

[42] A. R. Halpern, J. B. Wood, Y. Wang, and R. M. Corn, ACS Nano **8**, 1022 (2014).

[43] W. Srituravanich, N. Fang, C. Sun, Q. Luo, and X. Zhang, Nano Lett. **4**, 1085 (2004).

[44] K. A. Kouzakov and J. Berakdar, Phys. Rev. A **85**, 022901 (2012).

[45] N. J. M. Horing, E. Kamen, and H.-L. Cui, Phys. Rev. B **32**, 2184 (1985).

[46] C. Steinebach, D. Heitmann, and V. Gudmundsson, Phys. Rev. B **56**, 6742 (1997).

[47] B. P. van Zyl and E. Zaremba, Phys. Rev. B **59**, 2079 (1999).

[48] S. A. Mikhailov, Phys. Rev. B **58**, 1517 (1998).

[49] O. R. Matov, O. F. Meshkov, and V. V. Popov, J. Eur. Theor. Phys. **86**, 538 (1998).

[50] R. Roldan, M. O. Goerbig, and J.-N. Fuchs, Phys. Rev. B **80**, 085408 (2009).

[51] A. Politano, V. Formoso, and G. Chiarello, J. Phys.: Condens. Matter **25**, 345303 (2013).

[52] A. Politano and G. Chiarello, Carbon **71**, 176 (2014).

[53] O. V. Kibis, Phys. Rev. B **81**, 165433 (2010).

[54] M. Busl, G. Platero, and A.-P. Jauho, Phys. Rev. B **85**, 155449 (2012).

[55] K. A. Velizhanin and T. V. Shahbazyan, Phys. Rev. B **90**, 085403 (2014).